Soft-x-ray laser interferometry of a pinch discharge using a tabletop laser

C. H. Moreno,* M. C. Marconi,* K. Kanizay, and J. J. Rocca
Electrical Engineering Department, Colorado State University, Fort Collins, Colorado 80523

Yu. A. Uspenskii and A. V. Vinogradov
P. N. Lebedev Physical Institute, 53 Leninsky Prospekt, Moscow 117924, Russia

Yu. A. Pershin
Kharkov State Polytechnic University, 21 Frunze Street, Kharkov 310002, Ukraine
(Received 18 December 1998)

We have used a tabletop soft-x-ray laser and a wave-front division interferometer to probe the plasma of a pinch discharge. A very compact capillary discharge-pumped Ne-like Ar laser emitting at 46.9 nm was combined with a wave division interferometer based on Lloyd's mirror and Sc-Si multilayer-coated optics to map the electron density in the cathode region of the discharge. This demonstration of the use of tabletop soft-x-ray laser in plasma interferometry could lead to the widespread use of these lasers in the diagnostics of dense plasmas. [S1063-651X(99)12507-8]

PACS number(s): 52.70.La, 07.85.−m

I. INTRODUCTION

The ability to produce time-resolved two-dimensional maps of the electron density in dense plasmas is of major interest in understanding their dynamics, and validating and improving complex numerical plasma hydrodynamic codes. Interferometry with optical lasers has been widely utilized to map the electron density in numerous laser-created and discharge-created plasmas. However, free-free absorption and refraction of the probe beam by the plasma limit the maximum electron density and plasma size that can be probed with optical wavelengths. An additional limitation is imposed by the maximum number of fringe shifts ($\sim$50) that can be detected in practice [1]. Since all three of these limitations can be greatly reduced using a shorter wavelength probe beam, the extension of plasma interferometry to soft-x-ray wavelengths can significantly expand the maximum plasma densities and sizes that can be probed.

Soft-x-ray lasers have the brightness, monochromaticity, and spatial coherence necessary to conduct interferometry measurements in dense plasmas. The first soft-x-ray plasma interferometry experiments have made use of a 15.5-nm Ne-like Y soft-x-ray laser pumped by Nova, the world's most powerful laser [1,2]. In those pioneering experiments the soft-x-ray laser was combined with a Mach-Zehnder interferometer to probe high-density laser-created plasmas. That amplitude division interferometer was implemented utilizing thin multilayer beamsplitters and multilayer-coated mirrors developed for that wavelength. In those experiments the optical laser beam that pumps the soft-x-ray laser and the laser that produces the high-density plasma are produced by the same Nd:glass laser system (Nova) and, therefore, the soft-x-ray laser pulse and the plasma generation are perfectly synchronized, a situation that is ideal to probe the very dense plasmas that are produced at that large laser facility. However, the large size and low repetition rate of this type of soft-x-ray laser constitutes a limitation to its use in the study of other dense plasmas.

The important progress recently achieved in the development of tabletop soft-x-ray lasers creates new opportunities in the diagnosis of dense plasmas. A capillary discharge-pumped tabletop laser operating at 46.9 nm has been demonstrated to reach the saturation intensity [3]. A measurement of the spatial coherence of this laser showed that it exceeds the requirements to probe millimeter-size plasmas [4]. This laser can significantly extend the range of electron densities n_e and plasma sizes L that can be probed with tabletop lasers. For example, for a plasma with an electron temperature of 200 eV and $Z=15$, free-free absorption at 46.9 nm determines an optical depth of unity at $n_e^2 L = 5.8 \times 10^{41}\,\mathrm{cm}^{-5}$ [1]. In comparison, for the fourth harmonic of Nd-YAG ($\lambda = 0.265\,\mu$m), an optical depth of unity is reached at $n_e^2 L = 1.7 \times 10^{40}\,\mathrm{cm}^{-5}$. Therefore, if we consider a plasma with $n_e = 2 \times 10^{21}\,\mathrm{cm}^{-3}$ and allow for an attenuation of the probe beam of e^{-1}, the Ne-like Ar laser can be used to probe plasmas up to 1.45 mm in size, while a 0.265-μm beam allows probing of plasma sizes up to only $\approx$40 μm. Moreover, the smaller refraction angle of the 46.9-nm beam allows probing of plasmas with 30 times larger electron-density gradients. Several other relatively compact laser-pumped soft-x-ray lasers have also reached gain saturation [5], or are on the verge of reaching gain saturation and producing the output energies that will allow their use in plasma diagnostics [6,7]. These tabletop soft-x-ray lasers could be used to probe a great variety of dense plasmas. However, multilayer beamsplitters cannot be presently developed for the wavelengths corresponding to several of these lasers [3,6,8] due to the lack of materials with the adequate optical constants. This limits the implementation of amplitude division interferometers and requires the development of alternative interferometer configurations. Possible solutions include amplitude division interferometers schemes based on diffrac-

*Permanent address: Departamento de Fisica, Universidad de Buenos Aires, FCEyN, Buenos Aires, Argentina.

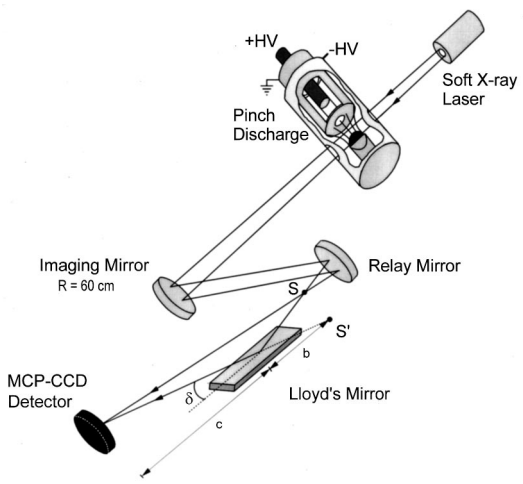

FIG. 1. Setup used for soft-x-ray interferometry of a pulsed discharge plasma.

tion gratings [9] and wave-front division interferometers [10,11]. Recently, a Fresnel bimirror wave-front division soft-x-ray interferometer was demonstrated and used in combination with a 21.2-nm Ne-like Zn laser to probe surface defects induced by an intense electric field [11].

We have recently demonstrated the use of a discharge-pumped 46.9-nm tabletop laser and a wave-front division soft-x-ray interferometer in plasma diagnostics [12]. The interferometer is based on Lloyd's mirror and recently developed Sc-Si multilayer mirrors having a normal incidence reflectivity of ≈34% at 46.9 nm. We have used these tools to map the electron density in the cathode region of a moderately dense pinch plasma with high spatial (≈10 μm) and temporal (0.6–0.7 ns) resolution. This experiment constitutes the demonstration of the use of a tabletop soft-x-ray laser and of a wave-front division interferometer in plasma diagnostics. In this paper we discuss all the aspects of this experiment, including the Lloyd's mirror interferometer, the development of the Sc-Si multilayer mirrors, the characterization of the discharge plasma, and present interferometry data. The next section describes the experimental aspects of this paper, and Sec. III discusses the results of the interferometry measurements.

II. EXPERIMENT

A schematic representation of the setup of the experiment is shown in Fig. 1. It comprises a tabletop capillary discharge laser that produces a $\lambda = 46.9$-nm probe beam, a capacitive discharge that generates the transient plasma that is the object of the study, and a wave-front division interferometer consisting of a grazing incidence mirror and two Sc-Si multilayer mirrors positioned at near-normal incidence. Each of the major components of the experiment are discussed below.

A. Tabletop capillary discharge Ne-like Ar laser

The soft-x-ray laser used in this experiment is a discharge-pumped collisionally excited Ne-like Ar tabletop laser emitting in a single line at 46.9 nm. It produces laser output pulses with energy of up to 25 μJ and of 0.6–0.8-ns duration [13]. Lasing is obtained by exciting a 4-mm diameter and a 16.4-cm-long polyacetal capillary filled with Ar gas at a pressure of about 600 mTorr with a fast current pulse. The current pulse that has a peak amplitude of about 37 kA and a first half-cycle duration of ≈72 ns is produced by discharging a Blumlein transmission line that uses water as dielectric. The transmission line is pulse-charged utilizing a compact Marx generator. The laser setup has a size comparable to many widely utilized visible and ultraviolet lasers and occupies a table area of about 0.4 m×1 m. The beam divergence is about 5 mrad at the discharge operating conditions used in the experiment [14]. In a previous experiment we have determined that the output of this laser is spatially coherent within a cone that has a full angle of 0.5–0.8 mrad [4].

B. Lloyd's mirror interferometer

Lloyd's mirror is the simplest possible wave-front division interferometer [15]. In this interferometer scheme an elongated mirror is positioned at grazing incidence to intercept and redirect part of a beam originated from a coherent source S. The part of the beam reflected by the mirror is made to overlap with the rest of the beam onto a detector screen where the interference pattern is observed. The spacing of the interference fringes in the detector plane ΔI is a function of the distance b between the source S and a generic location on the Lloyd's mirror surface, the distance c between that location and the detector screen, and the distance $d = 2b \sin\delta$ between S and its virtual image S' created by the Lloyd's mirror (where δ is the grazing angle of incidence of the radiation on the mirror surface):

$$\Delta I = \frac{(b+c)\lambda}{d} = \frac{(b+c)\lambda}{2b \sin\delta}, \tag{2.1}$$

It should be noted that in selecting the interfringe separation there is not complete freedom in the choice of the grazing incidence angle δ because in combination with the length of the Lloyd's mirror this angle also determines the maximum transverse size of the region that can be probed. Figure 2 illustrates the combination of fringes density and maximum transverse plasma sizes that are accessible for probing by changing δ for several mirror lengths between 10 and 25 cm. It was assumed that the soft-x-ray laser beam is coherent within a cone of 0.7-mrad full angle, and that the parameters of the interferometer correspond to the implementation described below. It was also assumed that the edge of the mirror is positioned to intercept the axis of the beam. Starting at $\delta = 0$, both the fringe density and the size of the probe region increase as a function of δ up to $\delta \approx 0.1-0.2$ mrad depending on the mirror length. At this point a further increase in the grazing incidence angle continues to enlarge the fringe density but causes a decrease of the size of the region that can be probed due to a decrease in the overlap between the reflected beam and the rest of the beam. For example, the computations show that under these conditions, a mirror length of 20 cm allows the probing of a transverse plasma size of 300 μm with a fringe density of 22 mm^{-1} at the object plane. In practice the useful size of the region of the interference fringes is somehow reduced by the appearance of diffraction fringes caused by the interception of the beam with the edge

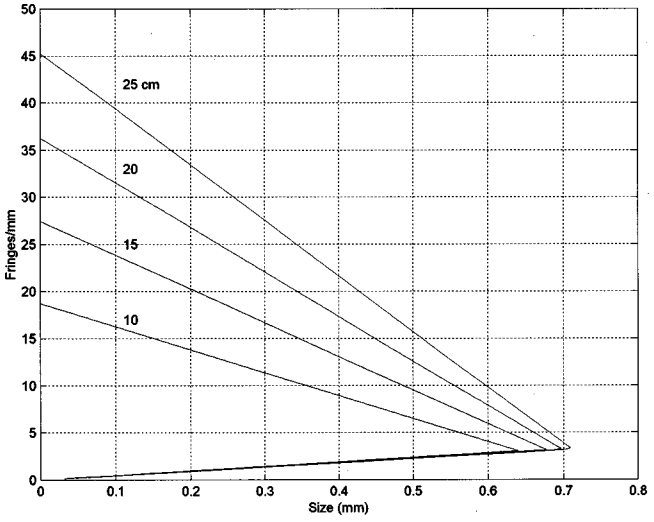

FIG. 2. Computed fringe density vs maximum transverse plasma sizes that are accessible for probing for mirror lengths between 10–25 cm. It was assumed that the soft-x-ray laser beam is coherent within a cone of 0.7-mrad full angle. The edge of the Lloyd mirror is assumed to intercept the axis of the beam. The parameters of the interferometer correspond to the implementation described in the text.

of the Lloyd's mirror. Nevertheless, a moderate increase of the size of the probed region with respect to that shown in Fig. 2 can be obtained by positioning the edge of the mirror off axis. This was the situation of our experiment in which we probed a region of $\approx 400\ \mu$m with a fringe density of 26 mm^{-1}.

The plasma under study is positioned to intercept about half of the laser beam, leaving the rest of it practically unperturbed. The plasma introduces a number of fringe shifts N in the probe beam that is related to the electron density n_e by

$$N = \int_0^L \frac{\Delta \eta}{\lambda} dx \approx \frac{L}{2\lambda} \frac{n_e}{n_{ec}}, \tag{2.2}$$

where x is measured along the probe beam, L is the plasma length along the path of the probe beam, and η is the index of refraction of the plasma, which in turn relates to the electron density n_e as $\eta = (1 - n_e/n_{ec})^{1/2}$, where $n_{ec} = 5 \times 10^{23}\,\mathrm{cm}^{-3}$ is the critical electron density for the propagation of the 46.9-nm laser probe radiation through the plasma. Consequently, n_e can be readily inferred by measuring $\Delta\Phi$, if the plasma length L is known.

In our experiment the point source S was obtained by focusing the laser beam with a concave Sc-Si multilayer mirror having a radius of curvature $R = 60\,\mathrm{cm}$. This concave mirror also images the plasma onto the detector plane. The Lloyd's mirror was obtained by cleaving a 2.5-cm×18-cm strip from a polished silicon wafer. The plasma was positioned at 2.4 m from the exit of the laser, where the beam has a spatial coherence length of at least 1.2 mm. The distance between the curved mirror and the plasma was 31.4 cm, and the distance between the curved mirror and the detector screen was 676 cm. A flat Sc-Si multilayer mirror was used to relay the image onto the detector. This optical setup projects onto the detector plane a real image of the plasma with 21.5× magnification. The detector consisted of a multichannel plate (MCP) followed by a phosphor screen, an image intensifier, and a 1024×1024 charge-coupled device (CCD) array. The MCP was gated during ≈5 ns to eliminate the background signal caused by the long-lasting (>300 ns) self-emission of the plasma. Also, the phosphor screen was coated with a thin aluminum film to reduce the background signal caused by visible plasma radiation. The Lloyd's mirror was positioned at a grazing angle of incidence of about 1.4 mrad, that determined an interfringe separation of 32 channels on the CCD corresponding to a fringe density of $\approx 26\ \mathrm{mm}^{-1}$ on the object plane.

C. Multilayer mirrors

The interferometer design requires the use of two near-normal incidence mirrors. The literature indicates that Ir or Os coatings can produce normal incidence reflectivities of nearly 20% at 46.9 nm [16]. However, we have observed during our experiments that in practice the reflectivity of Ir coatings deposited by electron-beam evaporation on superpolished surfaces is only ≈10% at this wavelength, which in our setup that uses two near-normal incidence mirrors reduces the intensity of the probe beam reaching the detector by nearly two orders of magnitude. To obtain a significant improvement in the throughput of the interferometer we designed and manufactured multilayer coatings optimized for maximum reflectivity at this wavelength. In plasma interferometry experiments the narrower bandwidth of these optimized multilayer mirrors also provides the important additional advantage of an increased contrast between the reflected probe beam and reflected plasma self-emitted radiation. Soft-x-ray multilayer coatings made of multiple pairs (periods) of absorber/spacer materials such as Mo-Si, Cr-C, and Cr-Sc have been extensively used as reflectors in the 10–30-nm spectral region for nearly 20 years. However, the choice of the best partner materials for the fabrication of reflective multilayers at 46.9 nm is not clearly evident. All the previously developed multilayer coatings, including Mo-Si and $MoSi_2$-Si, have very low reflectivity at 46.9 nm [17,18]. Under these circumstances the identification of the optimum material combination is key to the design of high reflectivity coatings at the wavelength of interest. We chose the Sc-Si combination in view of the following: Si is one of the best spacer materials for this wavelength due to its low absorption, and also the technology for its deposition into thin layers is well developed. The remarkable feature of Sc as an absorber material for this wavelength region is its high refractive index originating from very intense transitions of the $3p$ core electrons to the practically unoccupied $3d$ band ($3p^6 4s^2 3d^1 \rightarrow 3p^5 4s^2 3d^2$ transitions), which starts at $\lambda \approx 35\,\mathrm{nm}$. In addition, Sc has low absorption because of the small number of valence electrons in $4s$ and $3d$ shells and the low values of the cross sections of valence photo excitations at $\lambda = 46.9\,\mathrm{nm}$. For our numerical calculations the optical constants for Si were obtained from the literature, while those for Sc were obtained from *ab initio* calculations [19]. The theoretical results show that a perfect Sc-Si multilayer would have normal incidence reflectivity as high as 67% at $\lambda = 46.9\,\mathrm{nm}$.

A series of concave Sc-Si multilayer mirrors having a period $H = 18-27\,\mathrm{nm}$ were fabricated on superpolished sub-

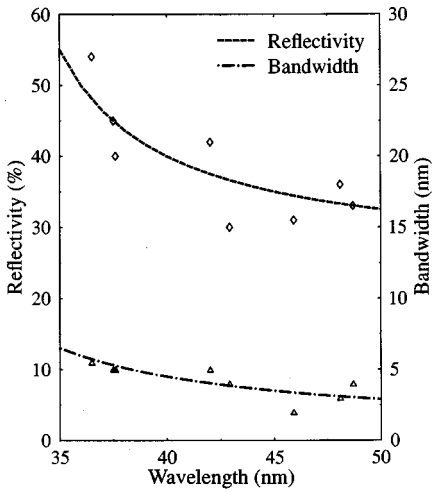

FIG. 3. Measured peak reflectivity ($\diamond$, left axis), and bandwidth ($\triangle$, right axis) of the Sc-Si mirrors as a function of the wavelength. The curves are smooth fits to the data points.

strates (surface rms roughness ≈ 1 Å) by dc-magnetron sputtering at 3×10^{-3} Torr of Ar. The multilayer coatings consisted of 10 periods, with a ratio of layer thicknesses $H(\mathrm{Sc})/H(\mathrm{Si})=0.7-0.8$ and a 2–4-nm-thick protective layer of Si on the top. The sputtering rate was 0.2–0.3 nm/s for the Sc layers and 0.4–0.5 nm/s for the Si layers. We found the substrate material (float glass, fused quartz, or silicon wafers) does not significantly affect the performance of the multilayers. In contrast, the use of electron-beam evaporation instead of magnetron sputtering results in strong deterioration of the quality of the multilayers. The normal incidence reflectivity of the Sc-Si concave mirrors was measured with 10% relative error by comparison of the intensity of the spectra of a laser plasma source (laser parameters: $\lambda=1.06\,\mu$m, 0.1 J, 5 ns, 1-mm diameter focal spot, and 1 Hz) with that of the plasma image produced using the multilayer mirror under investigation [20]. Figure 3 illustrates the results of reflectivity measurements for eight Sc-Si multilayer mirrors. At our working wavelength of 46.9 nm the normal incidence reflectivity and bandwidth of the mirrors are $\approx$34% and 4 nm, respectively (far right point on the curves of Fig. 3). These reflectivity data were confirmed in two independent measurements carried out at the BESSY synchrotron (Berlin) and at the Center for x-ray Optics (Berkeley, USA) [21]. Moreover, we verified that this relatively high reflectivity is maintained several months after fabrication and exposure to the atmosphere. The period and structure of the multilayers were tested using CuK_α and CoK_α ($\lambda=0.154$ and 0.179 nm) x-ray reflectometry at small and large angles as well as cross-sectional electron microscopy. These measurements allowed us to estimate the interface roughness of the fabricated mirrors to be $\sigma\approx1.1-1.3$ nm. An electron microscopy study of the cross section of the multilayers revealed regions of a mixed composition with a width of 3 nm at all Sc-Si and Si-Sc interfaces. Heating of the multilayer up to 670 °K was observed to lead to strong intermixing of Si and Sc layers and to precipitation of the $\mathrm{Sc_3Si_5}$ compound. Annealing at temperatures above 770 °K resulted in complete degradation of the multilayer structure. We believe that these interface processes are the main causes of the large difference between the calculated and observed reflectivity of the Sc-Si mirrors. Also, it is probable that some of the irregularities in the dependence of optical characteristics on a wavelength observed in Fig. 3 are connected with these processes. Nevertheless, the fabricated Sc-Si multilayer mirrors provide approximately 300% improvement in the normal incidence reflectivity available in practice for interferometry experiments with the 46.9-nm laser. Moreover, our studies show that the Sc-Si mirrors have a large potential for still further improvements of the reflectivity at 30–50 nm, and that they have a significant thermal stability that will allow their use in controlling rather intense soft-x-ray beams. More details about the Sc-Si multilayer mirrors can be found in Refs. [21, 22].

D. Pulsed discharge

The plasma that was the object of this paper was formed by means of a pulsed capacitive discharge, utilizing the electrode configuration schematically illustrated in Fig. 1. The plasma formation was initiated by a predischarge between the electrode identified as +HV in Fig. 1 and a grounded cylindrical stainless steel electrode placed at the opposite end of a 4-mm diameter channel in polyacetal. Material ablated from the walls of this channel was injected through a hole in the grounded electrode into the 4-mm gap between this electrode and a knife-edged cathode. These two electrodes were connected to a 3.2-μF capacitor charged to 12 kV. The capacitor was discharged through a spark-gap switch to excite the plasma that was formed from the material supplied by the auxiliary predischarge and material vaporized from the cathode by the discharge current pulse. The cathode was supported by a stainless steel cylinder that surrounded the plasma providing a return path for the current and partial protection for the mirrors from ablated electrode material. This coaxial electrode geometry allows for a relatively low inductance current path, which resulted in a current pulse of $\approx$30-kA peak amplitude and 1.8-μs half-period. The cathode was made of either stainless steel or copper. In both cases the cathode had a knife-edge profile with an edge length of 5 mm placed in the direction parallel to the propagation of the laser beam. This electrode geometry allowed for the creation of an elongated plasma in the direction of the probe beam. While both cathodes had similar shapes the stainless steel cathode had corners at the extremes of the knife edge with a smaller radius.

The magnetic force of the current pulse compresses the plasma, resulting in the formation of a moderately dense pinch that can be identified by the emission of a relatively short burst of short wavelength radiation ($\approx$150-ns full width at half maximum duration). The size, composition, temperature and temporal behavior of the plasma were characterized utilizing several diagnostic techniques. A vacuum photodiode with an aluminum photocathode was used to monitor the temporal evolution of the soft-x-ray emission from the plasma in every shot. Figure 4 shows the evolution of the photodiode signal in relation to the discharge current pulse. The pinch occurrence can be recognized by the pronounced peak on the photodiode signal, which in this shot takes place about 1 μs after the onset of the discharge current. Significant shot to shot variations in the time and amplitude of the

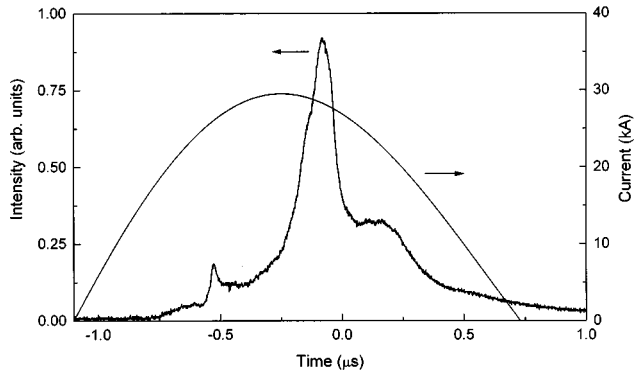

FIG. 4. Pulsed discharge plasma characteristics: discharge current pulse and temporal evolution of the vuv/soft-x-ray radiation emitted by the plasma.

radiation intensity were observed. The length of the plasma along the path of the probe beam was estimated from the extent of the vacuum ultraviolet/soft-x-ray emitting region of the plasma. The size of the vuv/soft-x-ray emitting region was determined in an auxiliary experiment in which the plasma was imaged onto the gated MCP-CCD detector with $4.3\times$ magnification using an iridium-coated spherical mirror with a 60-cm radius of curvature. Figure 5 shows an image corresponding to a discharge conducted using the copper cathode. As also observed for the discharges with the stainless steel cathode, the vuv/soft-x-ray emission is concentrated in the vicinity of the cathode. The silhouette of the cathode can be seen on the right side of the image partially covered by plasma. Although the pinch characteristics change significantly from shot to shot the plasma depth along the laser beam path was estimated to be (2.2 ± 0.5) mm and (1.9 ± 0.3) mm for the discharges that made use of the stainless steel cathode or copper, respectively.

The composition and degree of ionization of the plasma in the region near the cathode was inferred from the spectral

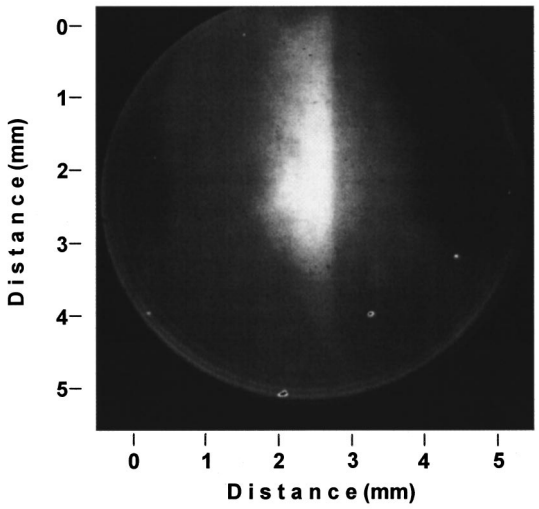

FIG. 5. Two-dimensional image of the pulsed discharge cathode region for a copper cathode. The anode is located towards the left side of the image and falls outside of the area of view. In the interferometry measurements the probe beam propagates along a vertical line and the Lloyd's mirror has its reflecting surface parallel to the plane of the figure.

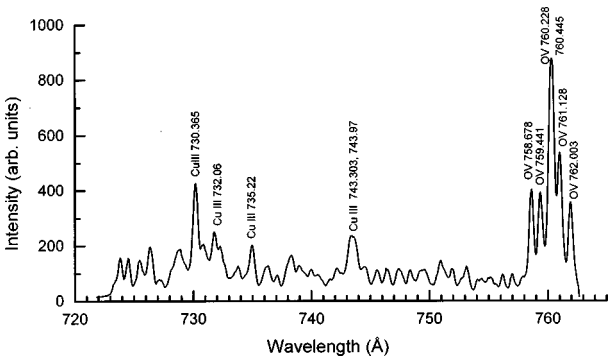

FIG. 6. Emission spectrum of the cathode region of the pulsed discharge using a copper cathode.

distribution of the plasma radiation. For this purpose, the plasma was imaged on to the slit of a spectrometer using an iridium-coated mirror with a radius of curvature of 60 cm. The plasma emission in the 50–120-nm spectral region was measured using a 1-m focal length normal incidence vacuum spectrometer provided with a 1200 lines-per-mm grating and a gated MCP-CCD detector. Spectra obtained for discharges with copper and stainless steel cathodes show that the plasma contains ions arising from the vaporization of cathode material by the current pulse and O ions and C ions corresponding to material ablated from the polyacetal walls of the channel of the predischarge. As an example, Fig. 6 shows a spectra corresponding to a discharge with the copper cathode. The spectra is dominated by O V and Cu III lines. Spectra obtained at other wavelengths also show lines of Cu IV, O III, and O IV. Spectra corresponding to discharges with the stainless steel cathode are also observed to contain lines of ions originated from cathode material, such us Fe III, Cr IV, and Ni III. The presence of strong O V lines indicates that in the region of interest the electron temperature is of the order of 10 eV and that all the atoms are ionized. The observation of metal vapor ions and strongest plasma self-emission near the cathode suggest that material ablated from the cathode makes an important contribution to the plasma.

III. INTERFEROGRAMS AND CONCLUSION

Soft-x-ray interferograms of plasmas generated using the stainless steel and copper cathodes are shown in Figs. 7 and 8, respectively. Figures 7(a) and 8(a) show the interference pattern obtained when no plasma was present. The shadow of the corresponding cathodes can be seen on the right side of each image. Uniformly spaced interference fringes with good contrast corresponding to a fringe visibility of $\approx 40\%$ can be observed in the central region of the images. The unevenly spaced fringes that appear at the bottom of Figs. 8(a) and 8(b) are diffraction fringes produced by the Lloyd's mirror edge. Figures 7(b) and 8(b) show interferograms produced when the plasma was present. Although the fringe contrast is degraded by the plasma self-emission, fringe shifts are clearly distinguishable in the vicinity of the cathodes. Three-dimensional maps of the electron-density distributions that result from analyzing these interferograms are shown in Figs. 7(c) and 8(c). Contour lines of the respective electron-density distributions are also displayed at the bottom of each figure. The dark contours show the relative position of the cathode electrodes. The analysis assumes the

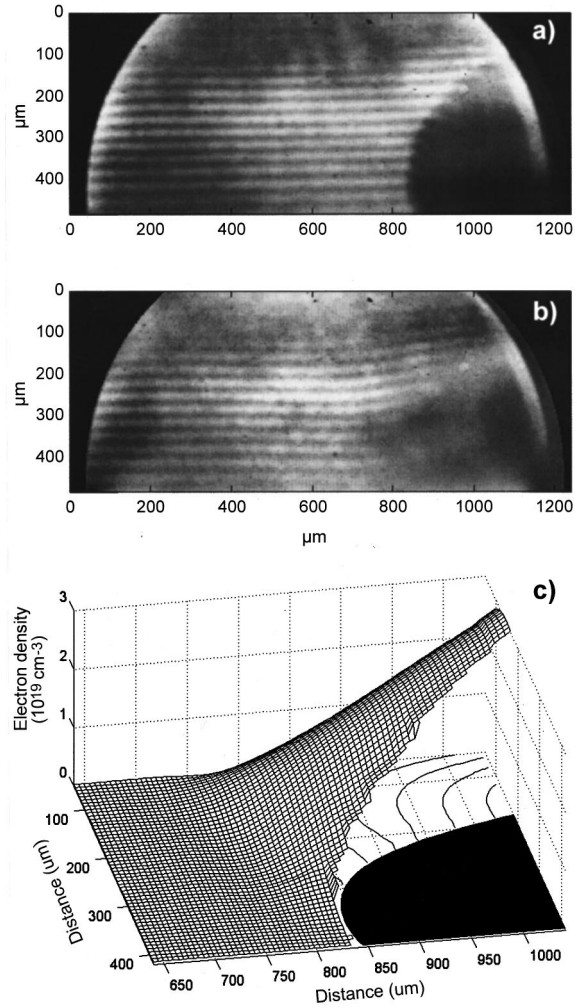

FIG. 7. Interferograms corresponding to a discharge with a stainless steel cathode. (a) Reference interferogram (no plasma present). The shade at the right is caused by the cathode electrode. (b) Interferogram with the plasma present. (c) Corresponding bidimensional distribution of the electron density. The dark contour shows the position of the cathode.

plasma is uniform in the direction of the probe beam. The elongated shape of the plasma along the cathode's edge (see Fig. 5) and the relatively uniform intensity of soft-x-ray self-emission along the probe path provide justification to this approximation.

In both cases the highest plasma density is observed to occur in the vicinity of the cathode. In the discharge shot corresponding to the stainless steel cathode the electron density reaches a maximum value of $(3.1\pm0.3)\times10^{19}\,\mathrm{cm}^{-3}$ in a region very close to the cathode surface. The electron density diminishes smoothly towards the anode. In the discharge shot corresponding to the copper electrode the highest density region of the plasma is observed to be concentrated within 300 μm off the cathode. The electron density reaches a maximum value of $(0.95\pm0.30)\times10^{19}\,\mathrm{cm}^{-3}$; at about 120 μm from the cathode surface. The significant supply of metal vapor from cathode ablation and the concentration of the current in the knife edge contribute to the creation of this significantly denser plasma region near the cathode. The regions of high electron density correspond well to those observed to yield maximum vuv/soft-x-ray self-emission. The

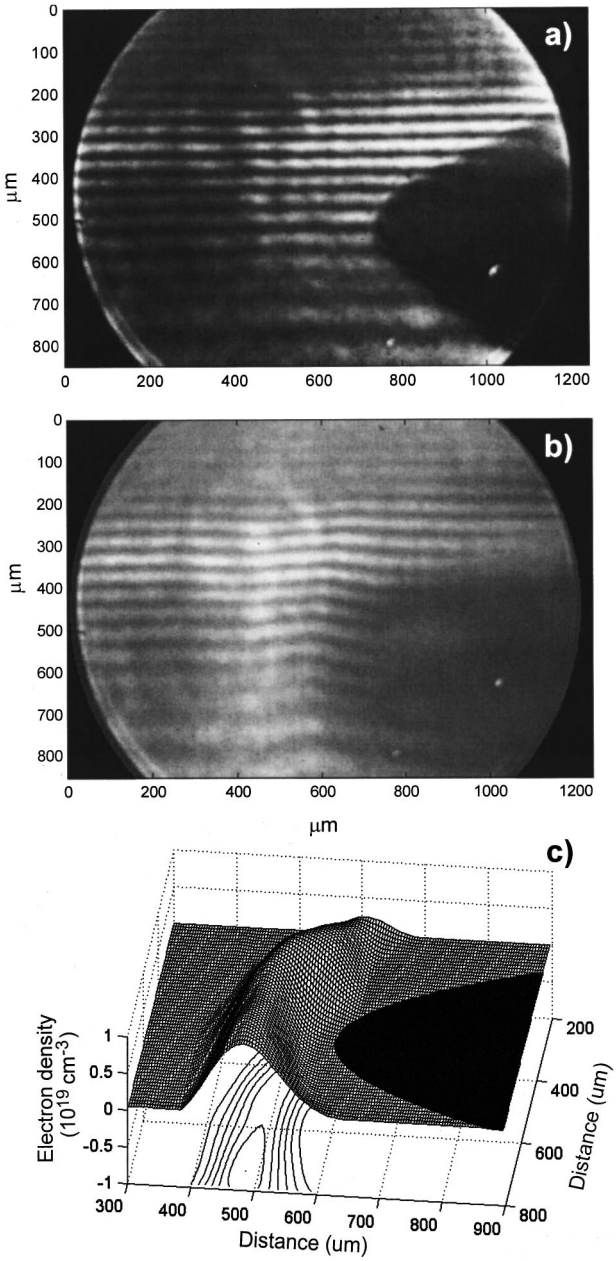

FIG. 8. Interferograms corresponding to a discharge with a copper cathode. (a) Reference interferogram (no plasma present). The shade at the right is caused by the cathode electrode. (b) Interferogram with the plasma present. (c) Corresponding bidimensional distribution of the electron density. The dark contour shows the position of the cathode. The relative time at which the interferogram was recorded with respect to the current pulse and the peak of the plasma self-emission is indicated as $t=0$ in Fig. 4. The probe beam and the cathode knife edge are parallel to the vertical axis.

absence of visible distortion of the fringes at distances greater than 300 μm from the cathode confirms that the plasma density is much lower in that region.

In summary, the results reported in this paper demonstrate the feasibility of conducting soft-x-ray interferometry with a tabletop soft-x-ray laser and the use of a wave-front division interferometer in plasma diagnostics. The results also illustrate that the development of high-reflectivity multilayer optics in the 30–50-nm wavelength region will allow the use of these tabletop short wavelength lasers in a variety of appli-

cations, including the diagnostics of a great variety of dense laboratory plasmas.

ACKNOWLEDGMENTS

This work was supported by U.S. DOE Grant No. DE-FG03-98DP00208. We acknowledge the collaboration of B. Benware and D. Burd in the development of the tabletop soft-x-ray laser. The development of the laser was supported by the National Science Foundation. We also acknowledge the support of CRDF Grant No. RP1-240 for the collaboration that allowed the development of the Sc-Si multilayer mirrors.

[1] L. B. Da Silva, T. W. Barbee, Jr., R. Cauble, P. Celliers, D. Ciarlo, S. Libby, R. A. London, D. Matthews, S. Mrowka, J. C. Moreno, D. Ress, J. E. Trebes, A. Wan, and F. Weber, Phys. Rev. Lett. **74**, 3991 (1995).

[2] A. S. Wan, T. W. Barbee, Jr., R. Cauble, P. Celliers, L. B. Da Silva, J. C. Moreno, P. W. Rambo, G. F. Stone, J. E. Trebes, and F. Weber, Phys. Rev. E **55**, 6293 (1997).

[3] J. J. Rocca, D. P. Clark, J. L. A. Chilla, and V. N. Shlyaptsev, Phys. Rev. Lett. **77**, 1476 (1996).

[4] M. C. Marconi, J. L. A. Chilla, C. H. Moreno, B. R. Benware, and J. J. Rocca, Phys. Rev. Lett. **79**, 2799 (1997).

[5] R. Tomassini, F. Löwenthal, and J. E. Balmer, in *X-ray Lasers 1998*, Proceedings of the 6th International Conference on x-ray Lasers, Kyoto, Japan, edited by Y. Kato (Institute of Physics and Physical Society, London, in press).

[6] P. V. Nickles, V. N. Shlyaptsev, M. Kalashnikov, M. Schnurer, I. Will, and W. Sander, Phys. Rev. Lett. **78**, 2748 (1997).

[7] J. Dunn, A. L. Osterheld, R. Shepherd, W. E. White, V. N. Shlyaptsev, and R. E. Stewart, Phys. Rev. Lett. **80**, 2825 (1998).

[8] F. G. Tomasel, J. J. Rocca, V. N. Shlyaptsev, and C. D. Macchietto, Phys. Rev. A **55**, 1437 (1997).

[9] J. L. A. Chilla, J. J. Rocca, O. E. Martinez, and M. C. Marconi, Opt. Lett. **21**, 955 (1996).

[10] J. Svatos, D. Joyeux, D. Phalippou, and F. Polack, Opt. Lett. **18**, 1367 (1993).

[11] F. Albert, D. Joyeux, P. Jaegle, A. Carillon, J. P. Chauvineau, G. Jamelot, A. Klisnick, J. C. Lagron, D. Phalippou, D. Ros, S. Sebban, and P. Zeitoun, Opt. Commun. **142**, 184 (1997).

[12] J. J. Rocca, C. H. Moreno, M. C. Marconi, and K. Kanizay, Opt. Lett. **24**, 420 (1999).

[13] B. R. Benware, C. H. Moreno, D. J. Burd, and J. J. Rocca, Opt. Lett. **22**, 796 (1997).

[14] C. H. Moreno, M. C. Marconi, V. N. Shlyaptsev, B. R. Benware, C. D. Macchietto, J. L. A. Chilla, J. J. Rocca, and A. Osterheld, Phys. Rev. A **58**, 1509 (1998).

[15] M. Born and E. Wolf, *Principles of Optics*, 5th ed. (Pergamon Press, Oxford, 1975).

[16] D. L. Windt, Ph.D. thesis, University of Colorado, Boulder, 1987 (unpublished).

[17] E. Spiller, *Soft X-Ray Optics* (SPIE Optical Engineering, Washington, DC, 1994).

[18] I. V. Kozhevnikov, L. L. Balakireva, A. I. Fedorenko, I. A. Kopealets, V. E. Levashov, A. N. Stetsenko, I. I. Struk, and A. V. Vinogradov, Opt. Commun. **125**, 13 (1996).

[19] Yu. A. Uspenskii, S. V. Antonov, V. Yu. Fedotov, and A. V. Vinogradov, Proc. SPIE **3156**, 288 (1997).

[20] S. S. Borisova, I. V. Kozhevnikov, V. V. Kondratenko, V. E. Levashov, I. I. Lyakhovskaya, I. F. Mikhailov, A. G. Ponomarenko, S. I. Sagitov, A. I. Fedorenko, V. A. Chirkov, and A. S. Shulakov, Zh. Tekh. Fiz. **59**, 78 (1989) [Sov. Phys. Tech. Phys. **34**, 298 (1989)].

[21] Yu. A. Uspenski, V. E. Levashov, A. V. Vinogradov, A. I. Fedorenko, V. V. Kondratenko, Yu. P. Pershin, E. N. Zubarev, S. Mrowka, and F. Schäffers, Nucl. Instrum. Methods Phys. Res. (to be published).

[22] Yu. A. Uspenski, A. V. Vinogradov, V. E. Levashov, A. I. Fedorenko, V. V. Kondratenko, Yu. P. Pershin, E. N. Zubarev, and V. Yu. Fedotov, Opt. Lett. **23**, 771 (1998).